

Pulse-Width Predictive Control for LTV Systems with Application to Spacecraft Rendezvous

R. Vazquez^{a,*}, F. Gavilan^a, E. F. Camacho^b

^a*Departamento de Ingeniería Aeroespacial. Escuela Superior de Ingenieros. Universidad de Sevilla, Camino de los Descubrimientos s/n, 41092, Sevilla, Spain*

^b*Departamento de Ingeniería de Sistemas y Automática. Escuela Superior de Ingenieros. Universidad de Sevilla, Camino de los Descubrimientos s/n, 41092, Sevilla, Spain*

Abstract

This work presents a model predictive controller (MPC) that is able to handle linear time-varying (LTV) plants with PWM control. The MPC is based on a planner that employs a PAM or impulsive approximation as a hot-start and then uses explicit linearization around successive PWM solutions for rapidly improving the solution by means of linear programming. As an example, the problem of rendezvous of spacecraft for eccentric target orbits is considered. The problem is modeled by the LTV Tschauner-Hempel equations, whose transition matrix is explicit; this is exploited by the algorithm for rapid convergence. The efficacy of the method is shown in a simulation study.

Keywords: Spacecraft autonomy, Space robotics, Pulse-width modulation, Trajectory planning, Optimal trajectory, Linear Time-Varying Systems.

1. Introduction

Aerospace systems often need to be controlled by using pulse-width modulated (PWM) actuators, i.e., actuators whose output level is fixed and can only be turned on and off, such as spacecraft thrusters. It would be therefore desirable to use control design methods that directly take into account pulsed actuators. However, most feedback design and motion planning methods ignore

*Corresponding author, Fax number +34954486041, Email address: rvazquez1@us.es
Email addresses: fgavilan@us.es (F. Gavilan), eduardo@esi.us.es (E. F. Camacho)

variable width pulses and approximate the control variables either by impulses (which produce instantaneous changes in some combination of the states) or pulse-amplitude modulated (PAM) control. However, neither impulsive actuation nor PAM actuation capture with precision the behavior of pulsed actuators such as spacecraft thrusters. A more realistic model has to take into account that, typically, thrusters are ON-OFF actuators, i.e., the thrusters are not able to produce arbitrary forces, but instead can only be switched on (producing the maximum amount of force) or off (producing no force). These switching times are the only signals that can be controlled. This type of control signal is usually referred to as Pulse-Width Modulated (PWM). Control design with PWM actuation poses a challenge because the system becomes nonlinear in the switching times, even if the system is linear.

One can find in the literature several procedures to find an equivalent PWM solution starting from a PAM solution (for instance in Shieh et al. (1996); Ieko et al. (1999); Bernelli-Zazzera et al. (1998)). These methods allow to, given the PAM inputs of a system, compute PWM inputs that produce a system output optimally approximating the output of the system when driven by the PAM signals. The results are based on the so-called Principle of Equivalent Areas, which computes the PWM signal so that it covers the same area as the PAM signal. However, while these procedures are quite effective in the sense that the output produced by the approximate PWM signals is very similar to the one produced by PAM signals, they assume that the plant is linear time-invariant.

In this paper, Model Predictive Control (MPC) is used to directly find PWM signals to control the system. MPC (see, e.g., Camacho and Bordons (2004)) is a family of methods that originated in the late seventies and has developed considerably since then. In MPC, the process model is used to predict the future plant outputs, based on past and current values and on the proposed optimal future control actions. These actions are calculated by the optimizer taking into account the cost function as well as the constraints. Since the plant is nonlinear in the control signals (ON-OFF times), the underlying optimization problem is nonlinear and possibly non-convex. To solve the problem, the algorithm starts

from an initial guess computed by solving an optimal linear program with PAM or impulsive actuation, approximate the solution with ON-OFF thrusters, and then iteratively linearize around the obtained solutions to improve the PWM solution. While the idea of linearization to specifically compute optimal PWM control signals in the context of MPC is, to the best knowledge of the authors, original, it must be noted that local linearization techniques have been used for optimal trajectory problems in other contexts (see e.g. Kim et al. (2002)).

As an application the problem of rendezvous of spacecraft is considered, i.e., the controlled close encounter of two space vehicles. Autonomous spacecraft rendezvous capabilities are becoming a necessity as access to space continues increasing. The field has become very active in recent years, with a rapidly growing literature. Among others, approaches based on trajectory planning and optimization (Breger and How (2008); Arzelier et al. (2013, 2011); Louembet et al. (2015); Deaconu et al. (2015, 2014); D’Amico et al. (2013); Gaias et al. (2014)) and predictive control (Richards and How (2003); Rossi and Lovera (2002); Asawa et al. (2006); Gavilan et al. (2009, 2012); Larsson et al. (2006); Hartley et al. (2012); Leomanni et al. (2014); Jewison et al. (2015); Weiss et al. (2012)) are emerging.

Classically, in these approaches the problem of rendezvous is modeled by using impulsive maneuvers; one computes a sequence of (possibly optimal) impulses (usually referred to as ΔV ’s) to achieve rendezvous.

Recently, Vazquez et al. (2011, 2014) introduced a trajectory planning algorithm for spacecraft rendezvous that was able to incorporate PWM control signals. The former considered the linear time-invariant Clohessy-Wiltshire model (target orbiting in a *circular* Keplerian orbit, see Clohessy and Wiltshire (1960)). The latter extended the approach to *elliptical* target orbits by using the linear time-varying Tschauner-Hempel model (see Tschauner and Hempel (1965)). Both methods start from an initial guess computed by solving an optimal linear program with PAM or impulsive actuation, approximate the solution with ON-OFF thrusters, and then iteratively linearize around the obtained solutions to improve the PWM solution. For both circular and elliptical target

orbits the algorithms are simple and reasonably fast, and simulations favorably compare with an impulsive-only approach. These results were extended in Vazquez et al. (2015) to a decreasing-horizon model predictive controller able to take into account orbital perturbations, disturbances or model errors.

In this paper, a *receding* horizon model predictive controller with PWM inputs is formulated for general LTV plants and both alternatives (PAM or impulsive starting guess) are discussed in detail, with an application to rendezvous given at the end of the paper.

The structure of the paper is as follows. In Section 2 the plant model is introduced. Three types of inputs are considered: PWM, PAM and impulsive. Section 3 follows with a formulation of the underlying optimization problem. Section 4 describes a method that solves the planning problem using PWM signals. Section 5 develops the model predictive controller. Next, Section 6 describes the application to spacecraft rendezvous. Section 7 presents a simulation study of the method applied to spacecraft rendezvous. The paper finishes with some remarks in Section 8.

2. System Model

Consider a linear time-varying system given as

$$\dot{x} = A(t)x + B(t)u, \tag{1}$$

where $x \in \mathbb{R}^n$ is the state, $u \in \mathbb{R}^m$ is the input (control) vector, and $A(t)$ and $B(t)$ are, respectively, $n \times n$ and $n \times m$ matrices depending on time $t \geq 0$.

Considering that, for some time $t_k \geq 0$, initial conditions $x(t_k) \in \mathbb{R}^n$ are given and the input is known, the solution to (1) for $t > t_k$ is given by

$$x(t) = \Phi(t, t_k)x(t_k) + \int_{t_k}^t \Phi(t, s)B(s)u(s)ds, \tag{2}$$

where $\Phi(t, t_k)$ is the *system transition matrix*, see for instance Rugh (1996). This matrix can be computed numerically (or analytically if possible) as the

unique solution to the linear matrix differential equation

$$\dot{\Phi}(t, t_k) = A(t)\Phi(t, t_k), \quad t > t_k \quad (3)$$

$$\Phi(t_k, t_k) = I. \quad (4)$$

To obtain an unified notation in term of the inputs, denote by $B_i(t)$ the i -th column of $B(t)$, corresponding to the i -th input $u_i(t)$, for $i = 1, \dots, m$. In the paper, time intervals starting at some initial time t_k and ending at $t_{k+1} = t_k + T$ are considered, where T will be an adequate sample time. Then equation (2) can be written as

$$x(t_{k+1}) = \Phi(t_{k+1}, t_k)x(t_k) + \sum_{i=1}^m \int_{t_k}^{t_{k+1}} \Phi(t_{k+1}, s)B_i(s)u_i(s)ds, \quad (5)$$

The objective is solving the problem with PWM inputs. In addition, two other types of inputs are considered; they will be used as an intermediate step towards computing PWM inputs by the algorithm. All types of input are analyzed in the following sections.

2.1. Pulse width-modulated (PWM) control

In the PWM case, each input u_i is a pulse starting at time $\tau_{k,i}$ (relative to t_k) with pulse width $\kappa_{k,i}$, with constant magnitude $u_{max} = u_{k,i}^W$, as shown in Fig. 1, i.e.,

$$u_i(t) = \begin{cases} 0, & t \in [t_k, t_k + \tau_{k,i}], \\ u_{k,i}^W, & t \in [t_k + \tau_{k,i}, t_k + \tau_{k,i} + \kappa_{k,i}], \\ 0, & t \in [t_k + \tau_{k,i} + \kappa_{k,i}, t_{k+1}], \end{cases} \quad (6)$$

with $\kappa_{k,i} > 0$, $\tau_{k,i} > 0$ and $\tau_{k,i} + \kappa_{k,i} < T$, where the last constraint prevent the PWM signal to spill over to the next time interval. Then, substituting $u_i(t)$ in (5) one obtains

$$x(t_{k+1}) = \Phi(t_{k+1}, t_k)x(t_k) + \sum_{i=1}^m \left(\int_{t_k + \tau_{k,i}}^{t_k + \tau_{k,i} + \kappa_{k,i}} \Phi(t_{k+1}, s)B_i(s)ds \right) u_{k,i}^W, \quad (7)$$

and denoting

$$B_{k,i}^W(\tau_{k,i}, \kappa_{k,i}) = \int_{t_k + \tau_{k,i}}^{t_k + \tau_{k,i} + \kappa_{k,i}} \Phi(t_{k+1}, s)B_i(s)ds, \quad (8)$$

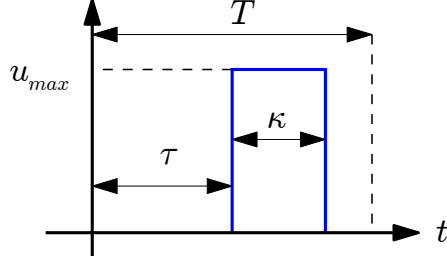


Figure 1: PWM Variables.

one can write the solution as

$$x(t_{k+1}) = \Phi(t_{k+1}, t_k)x(t_k) + \sum_{i=1}^m B_{k,i}^W(\tau_{k,i}, \kappa_{k,i})u_{k,i}^W. \quad (9)$$

There is an important difference between a PWM input and the PAM or impulsive inputs that will be subsequently introduced. While the latter can in principle take positive or negative values at different times, the former is fixed either as positive or negative for all time. Thus, typically a PWM model has twice number of inputs than a PAM/impulsive model. To make this explicit in the model (10), denote with a plus or minus super-index the positive or negative inputs, as follows

$$x(t_{k+1}) = \Phi(t_{k+1}, t_k)x(t_k) + \sum_{i=1}^m \left[B_{k,i}^W(\tau_{k,i}^+, \kappa_{k,i}^+)u_{k,i}^{W+} - B_{k,i}^W(\tau_{k,i}^-, \kappa_{k,i}^-)u_{k,i}^{W-} \right], \quad (10)$$

with $u_{k,i}^{W+}, \tau_{k,i}^+, \kappa_{k,i}^+$ and $u_{k,i}^{W-}, \tau_{k,i}^-, \kappa_{k,i}^-$ denoting, respectively, the magnitude, start, and width of the positive and negative i -th input pulses.

2.2. Pulse amplitud-modulated (PAM) control

In this case, each control $u_i(t)$ in (5) is constant inside the interval $[t_k, t_{k+1}]$, and equal to $u_{k,i}^A$. Then, substituting $u_i(t)$ in (5) one obtains

$$x(t_{k+1}) = \Phi(t_{k+1}, t_k)x(t_k) + \sum_{i=1}^m \left(\int_{t_k}^{t_{k+1}} \Phi(t_{k+1}, s)B_i(s)ds \right) u_{k,i}^A, \quad (11)$$

and denoting by

$$B_{k,i}^A = \int_{t_k}^{t_{k+1}} \Phi(t_{k+1}, s)B_i(s)ds, \quad (12)$$

the solution can be written as

$$x(t_{k+1}) = \Phi(t_{k+1}, t_k)x(t_k) + \sum_{i=1}^m B_{k,i}^A u_{k,i}^A. \quad (13)$$

2.3. Impulsive control

In this case, $u_i(t) = u_{k,i}^I \delta(t - (t_k + \tau_{k,i}))$, where $\delta(t)$ is Dirac's delta function, $t_k + \tau_{k,i}$ is the instant at which the impulse is given, and $u_{k,i}$ is the magnitude of the impulse. Then, assuming $0 < \tau_{k,i} < T$ for all i (all the impulses are given inside the considered time interval) and substituting $u_i(t)$ in (5) one obtains

$$x(t_{k+1}) = \Phi(t_{k+1}, t_k)x(t_k) + \sum_{i=1}^m \Phi(t_{k+1}, t_k + \tau_i) B_i(t_k + \tau_i) u_{k,i}^I, \quad (14)$$

and denoting by $B_{k,i}^I(\tau_{k,i}) = \Phi(t_{k+1}, \tau_i) B_i(t_k + \tau_i)$,

$$x(t_{k+1}) = \Phi(t_{k+1}, t_k)x(t_k) + \sum_{i=1}^m B_{k,i}^I(\tau_{k,i}) u_{k,i}^I. \quad (15)$$

2.4. Discretization and compact notation

Consider now a sequence of time instants $t_k = t_0 + kT$, $k = 0, \dots$, and denote $x_k = x(t_k)$. Then, it is possible to write, for both PAM and impulsive control,

$$x_{k+1} = A_k x_k + B_k U_k, \quad (16)$$

where $A_k = \Phi(t_{k+1}, t_k)$, and B_k and U_k depend on the input type. In the PWM case, write

$$x_{k+1} = A_k x_k + B_k^+ U_k^+ - B_k^- U_k^-, \quad (17)$$

where B_k^+ is a matrix whose i -th column is $B_{k,i}^W(\tau_{k,i}^+, \kappa_{k,i}^+)$ and U_k^+ , τ_k^+ , and κ_k^+ are column vectors whose i -th entries are, respectively, $u_{k,i}^W$, $\tau_{k,i}^+$ and $\kappa_{k,i}^+$. The same definitions (with minus super-index) are used for the negative pulses.

Then, to reach model (16), define

$$B_k = \begin{bmatrix} B_k^+ & -B_k^- \end{bmatrix}, U_k = \begin{bmatrix} U_k^+ \\ U_k^- \end{bmatrix}, \tau_k = \begin{bmatrix} \tau_k^+ \\ \tau_k^- \end{bmatrix}, \kappa_k = \begin{bmatrix} \kappa_k^+ \\ \kappa_k^- \end{bmatrix}. \quad (18)$$

The definitions of B_k are simpler for the other types of actuation. In the PAM case, B_k is a matrix whose i -th column is $B_{k,i}^A$ and U_k a column vector

whose i -th entry is $u_{k,i}^A$. In the impulsive case, B_k is a matrix whose i -th column is $B_{k,i}^I(\tau_{k,i})$, and U_k , τ_k are column vector whose i -th entries are, respectively, $u_{k,i}^I$ and $\tau_{k,i}$.

Next a compact formulation is developed to simplify the notation of the problem. The state at time t_{k+j+1} , given the state x_k at time t_k , and the input signals from t_k to time t_{k+j} , is computed by applying recursively, in the PAM and impulsive cases, by applying Equation (16):

$$x_{k+j+1} = A_{k+j+1,k}x_k + \sum_{i=k}^{k+j} A_{k+j,i}B_{k,i}U_{k,i}, \quad (19)$$

where the definition $A_{k,k} = \mathbf{I}$, $A_{k+1,k} = A_k$, and if $j > 0$ then $A_{k+j+1,k} = A_{k+j}A_{k+j-1} \dots A_k$ has been used. Define now \mathcal{X}_k and \mathcal{U}_k as a *stack vector* of N_p state and input vectors, respectively, spanning from time t_{k+1} to time t_{k+N_p} for the state and from time t_k to time t_{k+N_p-1} for the controls, where N_p is the planning horizon:

$$\mathcal{X}_k = \begin{bmatrix} x_{k+1} \\ \vdots \\ x_{k+N_p} \end{bmatrix}, \mathcal{U}_k = \begin{bmatrix} U_k \\ \vdots \\ U_{k+N_p-1} \end{bmatrix}.$$

Similarly, for the impulsive and PWM cases, define

$$\Gamma_k = \begin{bmatrix} \tau_k \\ \vdots \\ \tau_{k+N_p-1} \end{bmatrix}, \Lambda_k = \begin{bmatrix} \kappa_k \\ \vdots \\ \kappa_{k+N_p-1} \end{bmatrix}, \Upsilon_k = \begin{bmatrix} \Gamma_k \\ \Lambda_k \end{bmatrix}$$

Then one can write

$$\mathcal{X}_k = F_k x_k + G_k \mathcal{U}_k, \quad (20)$$

where G_k is a square, block lower triangular matrix of size mN_p , defined as

$$G_k = \begin{bmatrix} B_k & 0 & \cdots & 0 \\ A_{k+2,k+1}B_k & B_{k+1} & \cdots & 0 \\ \vdots & \vdots & \ddots & \vdots \\ A_{k+N_p,k+1}B_k & A_{k+N_p,k+2}B_{k+1} & \cdots & B_{k+N_p-1} \end{bmatrix}, \quad (21)$$

this is, its non-null blocks are defined by $(G_k)_{jl} = A_{k+j,k+l}B_{k+l-1}$, and the matrix F_k is defined as:

$$F_k = \begin{bmatrix} A_{k+1,k} \\ A_{k+2,k} \\ \vdots \\ A_{k+N_p,k} \end{bmatrix}. \quad (22)$$

It is important to note that, in the impulsive case, G_k is a (nonlinear) function of Γ_k , whereas in the PWM case it is a (nonlinear) function of Υ_k . To avoid lengthy expressions this dependence has been omitted. Another important remark is that, in the PWM case, \mathcal{U}_k is fixed whereas in the other cases is the input variable

3. Formulation of the planning problem

Next the planning problem is formulated, introducing the constraints and the objective function. The formulation is done for the three types of control signals.

3.1. Constraints on the problem

First constraints on the state and input are introduced. While only inequality are considered, equality constraints would be treated similarly.

3.1.1. Inequality constraints on the state

In this work it is assumed that the state is subject to inequality constraints along the planning horizon, which can vary as time advances. These can be formulated in general as $A_k \mathcal{X}_k \leq b_k$, and using (20), one reaches a expression in term of inputs, namely

$$A_k G_k \mathcal{U}_k \leq b_k - A_k F_k x_k. \quad (23)$$

3.1.2. Input constraints

Input constraints are different depending on the type of input.

In the PWM case, the inputs \mathcal{U}_k are fixed, but the start time of impulse, $t_k + \tau_k$, and its end, $t_k + \tau_k + \kappa_k$, must be within the time interval both for negative and positive pulses. Thus

$$0 \leq \Gamma_k, \quad (24)$$

$$0 \leq \Lambda_k, \quad (25)$$

$$\Gamma_k + \Lambda_k \leq T, \quad (26)$$

which can be summarized as

$$A^W \Upsilon_k \leq b^W. \quad (27)$$

In the PAM case, the inputs are limited above and below. Thus

$$\underline{U}_{PAM} \leq \mathcal{U}_k \leq \bar{U}_{PAM} \quad (28)$$

In the impulsive case, the inputs u_k are limited above and below, but also the times of impulse, $t_k + \tau_k$, must be within the time interval. Thus

$$\underline{U}_{IMP} \leq \mathcal{U}_k \leq \bar{U}_{IMP}, \quad (29)$$

$$0 \leq \Gamma_k \leq T. \quad (30)$$

3.2. Objective function

The objective function to be minimized in the planning problem is a combination of the 1-norm of the control signal, which is denote das $J_{\mathcal{U}}$, (which gives an estimation of fuel consumption in case the control signal is thrust, see Section 6) and a weighted 2-norm of the state, which is denoted as $J_{\mathcal{X}}$, both taken over the planning horizon. Thus,

$$J_k = J_{\mathcal{U},k} + \alpha J_{\mathcal{X},k}, \quad (31)$$

where α is a positive constant that allows us to give a relative weight between input cost and state error. $J_{\mathcal{X},k}$ is computed as

$$J_{\mathcal{X},k} = \mathcal{X}_k^T Q_k \mathcal{X}_k, \quad (32)$$

for $Q_k > 0$. Written in terms of the inputs and the starting point x_k , $J_{\mathcal{X},k}$ is

$$J_{\mathcal{X},k} = 2x_k^T F_k^T Q_k G_k \mathcal{U}_k + \mathcal{U}_k^T G_k^T Q_k G_k \mathcal{U}_k, \quad (33)$$

an expression in which the constant term $x_k^T F_k^T Q_k F_k x_k$, which does not play a role in the planning optimization as it is constant for a given x_k , is neglected.

The value of $J_{\mathcal{U},k}$ does, however, depend on the control type.

3.2.1. PWM control inputs

For the case of PWM control inputs, using definition (6) it can be seen that the objective function $J_U(k)$ is given by:

$$\begin{aligned} J_{\mathcal{U},k} &= \sum_{j=k}^{k+N_p-1} [(U_j^+)^T \kappa_j^+ + (U_j^-)^T \kappa_j^-] \\ &= \mathcal{U}_k^T \Lambda_k \\ &= A_k^J \Upsilon_k, \end{aligned} \quad (34)$$

with A_k^J defined by blocks as

$$A_k^J = \begin{bmatrix} 0 & 0 \\ 0 & U_k^T \end{bmatrix}. \quad (35)$$

The times Γ_k where inputs start does not play a role in the cost function (only their duration Λ_k).

3.2.2. PAM control inputs

For the case of PAM control inputs, it can be seen that the objective function $J_U(k)$ is given by:

$$J_{\mathcal{U},k} = \sum_{j=k}^{k+N_p-1} T \|U_j\|_1 = T \|\mathcal{U}_k\|_1. \quad (36)$$

3.2.3. Impulsive control inputs

For the case of impulsive control inputs, $J_U(k)$ is given by:

$$J_{\mathcal{U},k} = \sum_{j=k}^{k+N_p-1} \|U_j\|_1 = \|\mathcal{U}_k\|_1, \quad (37)$$

where it should be noticed that, as in the PWM case, the location $\tau_{k,i}$ of the impulses does not play a role in the cost function.

3.3. Planning optimization problem

Now, for each of the input types, one can formulate a planning optimization problem starting from initial condition x_k at time t_k , with a planning horizon of N_p , as follows.

3.3.1. PWM control inputs

For PWM control inputs, the planning optimization problem is formulated as

$$\begin{aligned} \min_{\Upsilon_k} \quad & 2x_k^T F_k^T Q_k G_k(\Upsilon_k) \mathcal{U}_k + \mathcal{U}_k^T G_k^T(\Upsilon_k) Q_k G_k(\Upsilon_k) \mathcal{U}_k + \alpha A_k^J \Upsilon_k, \\ \text{s. t.} \quad & A_k G_k(\Upsilon_k) \mathcal{U}_k \leq b_k - A_k F_k x_k. \end{aligned} \quad (38)$$

$$A^W \Upsilon_k \leq b^W. \quad (39)$$

Notice that \mathcal{U}_k is known, and one has to compute the start and width of the pulses, contained in Υ_k (start and duration of pulses), which enter nonlinearly in the optimization problem. The dependence of G_k on Υ_k has been made explicit.

3.3.2. PAM control inputs

For PAM control inputs, the planning optimization problem is formulated as

$$\begin{aligned} \min_{\mathcal{U}_k} \quad & 2x_k^T F_k^T Q_k G_k \mathcal{U}_k + \mathcal{U}_k^T G_k^T Q_k G_k \mathcal{U}_k + \alpha T \|\mathcal{U}_k\|_1, \\ \text{s. t.} \quad & A_k G_k \mathcal{U}_k \leq b_k - A_k F_k x_k. \\ & \underline{U}_{PAM} \leq \mathcal{U}_k \leq \bar{U}_{PAM}. \end{aligned} \quad (40)$$

3.3.3. Impulsive control inputs

For impulsive control inputs, the planning optimization problem is formulated as

$$\begin{aligned}
& \min_{\mathcal{U}_k, \Gamma_k} && 2x_k^T F_k^T Q_k G_k(\Gamma_k) \mathcal{U}_k + \mathcal{U}_k^T G_k^T(\Gamma_k) Q_k G_k(\Gamma_k) \mathcal{U}_k + \alpha \|\mathcal{U}_k\|_1, \\
\text{s. t.} & && A_k G_k(\Gamma_k) \mathcal{U}_k \leq b_k - A_k F_k x_k. \\
& && \underline{U}_{IMP} \leq \mathcal{U}_k \leq \bar{U}_{IMP}, \\
& && 0 \leq \Gamma_k \leq T.
\end{aligned} \tag{41}$$

The dependence of G_k on Γ_k (location of impulses) has been made explicit to emphasize that the optimization problem is nonlinear.

4. PWM planning algorithm

In this section the subindex k is kept even though it does not play any role. For a “pure” planning problem, it could be set to zero. However, k will be useful when defining the MPC algorithm in Section 5.

Consider now the problem (38), given x_k and \mathcal{U}_k . Since the problem is nonlinear, one needs to design an algorithm to solve it. The planning algorithm is based on starting the problem using either the impulsive or PAM model. The algorithm is composed of the following steps.

Step 1. Solve either the PAM optimization problem (40), or the impulsive problem (41) with a fixed Γ_k , to provide an initial guess of the PWM solution.

Step 2. The PAM or impulsive control inputs resulting from the optimization algorithm in Step 1 are converted to a sequence of PWM inputs, denote this initial sequence by Υ_k^0 . Set $i = 0$.

Step 3. The trajectory of the system with the PWM inputs Υ_k^i is computed analytically (if possible) or numerically by using equation (20). Denote the trajectory by \mathcal{X}_k^i .

Step 4. The system with PWM inputs is *linearized* around \mathcal{X}_k^i , thus obtaining a linear, explicit plant with respect to *increments*, denoted as Δ_k^i , in the PWM inputs. Then a quadratic program can be posed and solved to find the increments that improve the cost function.

Step 5. The resulting solution Δ_k^i is used to improve the approximation towards the real solution, by setting $\Upsilon_k^{i+1} = \Upsilon_k^i + \Delta_k^i$. Increase i by one and go back to Step 3. The process is iterated until the solution converges or time is up.

Next, all the steps in the algorithm are described.

4.1. Step 1. Computation of PAM/impulsive control input

First, one has to choose if to find an initial guess using a PAM approach or an impulsive approach. The PAM guess is more suitable if one expects wide pulses, whereas the impulsive guess is best when the pulses are rather short.

If a PAM guess is chosen, it is computed from (40), setting $\bar{U}_{IMP} = T\mathcal{U}_k^+$ and $\underline{U}_{IMP} = T\mathcal{U}_k^-$, so that the solution can always be converted to PWM following the procedure of Section 4.2. On the other hand, the impulsive guess is computed from (41), setting $\bar{U}_{IMP} = \mathcal{U}_k^+$ and $\underline{U}_{IMP} = \mathcal{U}_k^-$. The impulsive guess also requires to set the impulse location Γ_k to some pre-determined value, so only the impulse magnitude (which appears linearly in (41)) is unknown. Typical positions would be the middle of the interval (all entries of Γ_k equal to $T/2$) or start of the interval ($\Gamma_k = 0$).

4.2. Step 2. Initial PWM solution: Adapting the PAM/impulsive solution

The PAM/impulsive solution from Section 4.1, \mathcal{U} , is transformed to a PWM sequence of inputs, as follows:

1. From \mathcal{U} extract $u_{j,i}^A$ (or $u_{j,i}^I$ if the initial solution is of impulsive type) for $j = k, \dots, k + N_p - 1$ and $i = 1, \dots, m$. Also extract $\tau_{j,i}$ if the initial solution is of impulsive type.

2. If the initial solution is of PAM type, set

$$\tau_{j,i}^+(t) = \begin{cases} \frac{T u_{j,i}^A}{u_{j,i}^{W\pm}}, & u_{j,i}^A > 0, \\ 0, & u_{j,i}^A \leq 0, \end{cases} \quad \tau_{j,i}^-(t) = \begin{cases} -\frac{T u_{j,i}^A}{u_{j,i}^{W\pm}}, & u_{j,i}^A < 0, \\ 0, & u_{j,i}^A \geq 0, \end{cases} \quad (42)$$

and if the initial solution is of impulsive type,

$$\tau_{j,i}^+ = \begin{cases} \frac{u_{j,i}^I}{u_{j,i}^{W\pm}}, & u_{j,i}^A > 0, \\ 0, & u_{j,i}^I \leq 0, \end{cases} \quad \tau_{j,i}^- = \begin{cases} -\frac{u_{j,i}^I}{u_{j,i}^{W\pm}}, & u_{j,i}^A < 0, \\ 0, & u_{j,i}^I \geq 0, \end{cases} \quad (43)$$

3. In the PAM case, the PWM input should be centered in the interval: $\kappa_{j,i}^+ = \frac{T - \tau_{j,i}^+}{2}$, $\kappa_{j,i}^- = \frac{T - \tau_{j,i}^-}{2}$. In the impulsive case, the PWM input should be centered around the chosen $\tau_{j,i}$ (corrected if necessary to avoid spillover), i.e.

$$\kappa_{j,i}^+ = \begin{cases} 0, & \tau_{j,i} - \frac{\tau_{j,i}^+}{2} < 0, \\ T - \tau_{j,i}^+, & \tau_{j,i} + \frac{\tau_{j,i}^+}{2} > T, \\ \tau_{j,i} - \frac{\tau_{j,i}^+}{2}, & \text{otherwise,} \end{cases} \quad (44)$$

$$\kappa_{j,i}^- = \begin{cases} 0, & \tau_{j,i} - \frac{\tau_{j,i}^-}{2} < 0, \\ T - \tau_{j,i}^-, & \tau_{j,i} + \frac{\tau_{j,i}^-}{2} > T, \\ \tau_{j,i} - \frac{\tau_{j,i}^-}{2}, & \text{otherwise,} \end{cases} \quad (45)$$

4. From $\tau_{j,i}^+$, $\tau_{j,i}^-$, $\kappa_{j,i}^+$, and $\kappa_{j,i}^-$, construct Γ_k and Λ_k and thus Υ_k .

The PWM signals Γ_k, Λ_k constructed by this method produce a moderately similar (but not equal) output to the system driven by PAM or impulsive signals, but as time advances the output might considerably differ. See Shieh et al. (1996); Ieko et al. (1999); Bernelli-Zazzera et al. (1998) for more details and other methods. In addition, the PWM results are not optimal (with respect to the PWM signals) and they might not even verify the constraints. However, this solution is only used as an initialization for the optimization algorithm proposed next. Denote as Υ_k^0 the found solution and set $i = 0$.

4.3. Step 3. Computation of trajectories under PWM inputs

For the current iteration i , apply (20) to compute the states of the system \mathcal{X}_k^i at all times, with PWM inputs Υ_k^i . The matrix G_k might be needed to

compute numerically if an explicit solution for the integrals (10) is not known or possible.

4.4. Steps 4 and 5. Refined PWM solution: An optimization algorithm

To linearize (20) around inputs Υ_k^i , notice from (8) that

$$\begin{aligned} \frac{\partial}{\partial \tau_{k,i}} B_{k,i}^W(\tau_{k,i}, \kappa_{k,i}) &= \frac{\partial}{\partial \tau_{k,i}} \int_{t_k + \tau_{k,i}}^{t_k + \tau_{k,i} + \kappa_{k,i}} \Phi(t_{k+1}, s) B_i(s) ds, \\ &= \Phi(t_{k+1}, t_k + \tau_{k,i} + \kappa_i) B_i(t_k + \tau_{k,i} + \kappa_{k,i}) \\ &\quad - \Phi(t_{k+1}, t_k + \tau_{k,i}) B_i(t_k + \tau_{k,i}), \end{aligned} \quad (46)$$

and

$$\begin{aligned} \frac{\partial}{\partial \kappa_{k,i}} B_{k,i}^W(\tau_{k,i}, \kappa_{k,i}) &= \frac{\partial}{\partial \kappa_{k,i}} \int_{t_k + \tau_{k,i}}^{t_k + \tau_{k,i} + \kappa_{k,i}} \Phi(t_{k+1}, s) B_i(s) ds, \\ &= \Phi(t_{k+1}, t_k + \tau_{k,i} + \kappa_i) B_i(t_k + \tau_{k,i} + \kappa_{k,i}). \end{aligned} \quad (47)$$

Thus, (16) can be explicitly linearized around some given $\bar{\tau}_k^+$, $\bar{\tau}_k^-$ and $\bar{\kappa}_k^+$, $\bar{\kappa}_k^-$, reaching

$$x_{k+1} = A_k x_k + B_k U_k + B_k^{\Delta\tau} \delta\tau_k + B_k^{\Delta\kappa} \delta\kappa_k, \quad (48)$$

where B_k is computed with $\bar{\tau}_k^+$, $\bar{\tau}_k^-$, $\bar{\kappa}_k^+$, and $\bar{\kappa}_k^-$, and define

$$B_k^{\Delta\tau} = \begin{bmatrix} B_k^{\delta\tau^+} & B_k^{\delta\tau^-} \end{bmatrix}, \quad B_k^{\Delta\kappa} = \begin{bmatrix} B_k^{\delta\kappa^+} & B_k^{\delta\kappa^-} \end{bmatrix}, \quad (49)$$

$$\delta\tau_k = \begin{bmatrix} \bar{\tau}_k^+ - \tau_k^+ \\ \bar{\tau}_k^- - \tau_k^- \end{bmatrix}, \quad \delta\kappa_k = \begin{bmatrix} \bar{\kappa}_k^+ - \kappa_k^+ \\ \bar{\kappa}_k^- - \kappa_k^- \end{bmatrix}, \quad (50)$$

where the i -th entries of the B_k^δ matrices in (50) are given, respectively, by

$$\begin{aligned} (B_k^{\delta\tau^+})_i &= \Phi(t_k + T, t_k + \bar{\tau}_{k,i}^+ + \bar{\kappa}_{k,i}^+) B_i(t_k + \bar{\tau}_{k,i}^+ + \bar{\kappa}_{k,i}^+) u_{k,i}^{W+} \\ &\quad - \Phi(t_k + T, t_k + \bar{\tau}_{k,i}^+) B_i(t_k + \bar{\tau}_{k,i}^+) u_{k,i}^{W+} \end{aligned} \quad (51)$$

$$\begin{aligned} (B_k^{\delta\tau^-})_i &= -\Phi(t_k + T, t_k + \bar{\tau}_{k,i}^- + \bar{\kappa}_{k,i}^-) B_i(t_k + \bar{\tau}_{k,i}^- + \bar{\kappa}_{k,i}^-) u_{k,i}^{W-} \\ &\quad + \Phi(t_k + T, t_k + \bar{\tau}_{k,i}^-) B_i(t_k + \bar{\tau}_{k,i}^-) u_{k,i}^{W-} \end{aligned} \quad (52)$$

$$(B_k^{\delta\kappa^+})_i = \Phi(t_k + T, t_k + \bar{\tau}_{k,i}^+ + \bar{\kappa}_{k,i}^+) B_i(t_k + \bar{\tau}_{k,i}^+ + \bar{\kappa}_{k,i}^+) u_{k,i}^{W+}, \quad (53)$$

$$(B_k^{\delta\kappa^-})_i = -\Phi(t_k + T, t_k + \bar{\tau}_{k,i}^- + \bar{\kappa}_{k,i}^-) B_i(t_k + \bar{\tau}_{k,i}^- + \bar{\kappa}_{k,i}^-) u_{k,i}^{W-} \quad (54)$$

Thus, defining stack vectors with the increments in the PWM variables at step i as

$$\Delta\Gamma_k^i = \begin{bmatrix} \delta\tau_k \\ \vdots \\ \delta\tau_{k+N_p-1} \end{bmatrix}, \quad \Delta\Lambda_k^i = \begin{bmatrix} \delta\kappa_k \\ \vdots \\ \delta\kappa_{k+N_p-1} \end{bmatrix},$$

and grouping all increments as

$$\Delta_k^i = \begin{bmatrix} \Delta\Gamma_k^i \\ \Delta\Lambda_k^i \end{bmatrix}, \quad B_k^\Delta = \begin{bmatrix} B_k^{\Delta\tau} \\ B_k^{\Delta\kappa} \end{bmatrix},$$

and defining G_k^Δ as in (55), i.e.,

$$G_k^\Delta = \begin{bmatrix} B_k^\Delta & 0 & \cdots & 0 \\ A_{k+2,k+1}B_k^\Delta & B_{k+1}^\Delta & \cdots & 0 \\ \vdots & \vdots & \ddots & \vdots \\ A_{k+N_p,k+1}B_k^\Delta & A_{k+N_p,k+2}B_{k+1}^\Delta & \cdots & B_{k+N_p-1}^\Delta \end{bmatrix}, \quad (55)$$

one can write

$$\mathcal{X}_k^i \approx F_k x_k + G_k(\Upsilon_k^i)\mathcal{U}_k + G_k^\Delta(\Upsilon_k^i)\Delta_k^i, \quad (56)$$

The state constraints (85) become

$$A_k G_k^\Delta(\Upsilon_k^i)\Delta_k^i \leq b_k - A_k F_k x_k - G_k(\Upsilon_k^i)\mathcal{U}_k. \quad (57)$$

The constraints on $\Delta\Gamma_k^i$ and $\Delta\Lambda_k^i$ are as follows:

$$-A^W \Delta_k^i \leq b^W - A^W \Upsilon_k^i, \quad (58)$$

$$\Delta_{max} \leq \Delta_k^i \leq \Delta_{max}, \quad (59)$$

where the last constraint (59) is used to avoid large variations that might make the linearization approximation to fail. All these constraints are might be summarized as

$$A^\Delta \Delta_k^i \leq b^\Delta \quad (60)$$

Finally, the objective function can be rewritten in terms of Δ_k^i as $J_k^i = J_k^i(\Upsilon_k^i) + J_k^\Delta(\Upsilon_k^i, \Delta_k^i)$, where

$$J_k^i = 2x_k^T F_k^T Q_k G_k(\Upsilon_k^i) \mathcal{U}_k + \mathcal{U}_k^T G_k^T(\Upsilon_k^i) Q_k G_k(\Upsilon_k^i) \mathcal{U}_k + \alpha A_k^J \Upsilon_k^i, \quad (61)$$

$$J_k^\Delta = 2(x_k^T F_k^T + \mathcal{U}_k^T G_k^T(\Upsilon_k^i)) Q_k G_k^\Delta(\Upsilon_k^i) \Delta_k^i + (\Delta_k^i)^T G_k^{\Delta T}(\Upsilon_k^i) Q_k G_k^\Delta(\Upsilon_k^i) \Delta_k^i + \alpha A_k^J \Delta_k^i. \quad (62)$$

Noting that J_k^Δ is quadratic in Δ_k^i , a quadratic optimization program with linear restriction, formulated on the output increments, can be posed as follows:

$$\begin{aligned} \min_{\Delta_k^i} \quad & J_k^\Delta(\Upsilon_k^i, \Delta_k^i) \\ \text{s. t.} \quad & A_k G_k^\Delta(\Upsilon_k^i) \Delta_k^i \leq b_k - A_k F_k x_k - G_k(\Upsilon_k^i) \mathcal{U}_k, \\ & A^\Delta \Delta_k^i \leq b^\Delta. \end{aligned} \quad (63)$$

The solution Δ_k is used to recompute new PWM inputs, $\Upsilon_k^{i+1} = \Upsilon_k^i + \Delta_k^i$. Then the linearization process can be repeated around the new Υ_k^{i+1} , refining the solution in each iteration.

5. Model Predictive Control with PWM inputs

In this section, building upon the trajectory planning algorithm of Section 4, which is open-loop and has a finite time-horizon, a closed-loop algorithm is developed based on the ideas of model predictive control (also known as receding horizon control). Model predictive control closes the loop by simply re-planning the maneuver at each time step, after applying just the set of control inputs corresponding to the first time step, and keeps looking ahead N_p time steps. Thus, the algorithm starts at $k = 0$ and is repeated for each k . The re-planning is done from the actual position at each time step, which seldom coincides with the planned position due to disturbances, thus effectively closing the loop.

However, except at the start, it is not necessary to repeat all the steps of Section 4. Since the new position should be close to the planned one, one can apply the linearization scheme of the planning algorithm starting from the last available linearization. The MPC algorithm is summarized next:

Step 1. At time step $k = 0$ and starting from x_0 apply the Planning algorithm of Section 4, obtaining a set of PWM inputs Υ_0 that would optimize the planning problem (38) for the next N_p time steps, if there were no disturbances.

Step 2. Apply impulses corresponding to the first time instant; save the rest of impulses. Set $k = 1$

Step 3. One arrives at x_k , which probably is not the intended value of the state at time k but close. Thus re-planning is necessary.

Step 4. For re-planning, apply the planning algorithm of Section 4. However, to avoid the initial step of having to use a PAM or impulsive model and compute an initial guess, use instead as an initial guess the impulses of Υ_{k-1} that were not used (all of them except those corresponding to time $k - 1$) and guess the remaining impulses (at the end) as zeros. In this way, form an initial guess Υ_k^0 .

Step 4. Apply the linearization algorithm of Section 4.4 using Υ_k^0 as initial guess to obtain, after iterating, a new set of impulses Υ_k . Apply the set of impulses corresponding to time k . Save the rest of impulses.

Step 5. Repeat step 3.

6. Example application: Spacecraft Rendezvous

Rendezvous of spacecraft is the controlled close encounter of two (or more) space vehicles. This work assumes just two vehicles, one of which is the *target vehicle* (which is in a known orbit, and considered passive) and the other is the *chaser spacecraft*, which begins from a known position and maneuvers until very close to target. Only close range rendezvous Fehse (2003) is considered, which starts at hundreds of meters and ends when the chaser is very close to target (a few meters with speeds of centimeters per second).

There are numerous mathematical models for spacecraft rendezvous; which one should be used depends on the parameters of the scenario. In Carter (1998) a survey of numerous mathematical models for spacecraft rendezvous can be found.

For instance, if the target is orbiting in a *circular* Keplerian orbit, the general equations of the relative movement between an active chaser spacecraft close to a passive target vehicle are linear time-invariant Hill-Clohessy-Wiltshire (HCW) equations (introduced in Hill (1878) and Clohessy and Wiltshire (1960)). While these equations are frequently used in the literature, it must be noted that, in many situations, the HCW equations are not accurate. For instance, if the target vehicle is moving in a Keplerian *eccentric* orbit (see Inalhan et al. (2002)) or if some orbital perturbations are taken into account (see for example Humi and Carter (2008)). A more complex model, the Tschauner-Hempel model (see Tschauner and Hempel (1965) or Carter (1998)) assumes that the target vehicle is passive and moving along an elliptical orbit with semi-major axis a and eccentricity e . The system equations are linear time-varying and cannot be exactly integrated in time to obtain a discrete transition model; however, if one substitutes the time t by the *eccentric* anomaly of the target orbit, E , it is possible to obtain explicit expressions for the system evolution in the PWM, impulsive, and PAM actuation cases. This will be the model considered in this work. The model can be expressed in cartesian coordinates, but also in the so-called relative orbital elements (see, e.g., Gaias et al. (2014) or Sinclair et al. (2014)). The former has been chosen for simplicity.

Let us first establish some notation. Define the orbital mean motion $n = \sqrt{\frac{\mu}{a^3}}$, where μ is the gravitational parameter of the central body around which the target spacecraft is orbiting.

Now, note that t and E are related in a one-to-one fashion by using Kepler's equation:

$$n(t - t_p) = E - e \sin E, \quad (64)$$

where t_p is the time at periapsis used as a starting point to measure the ec-

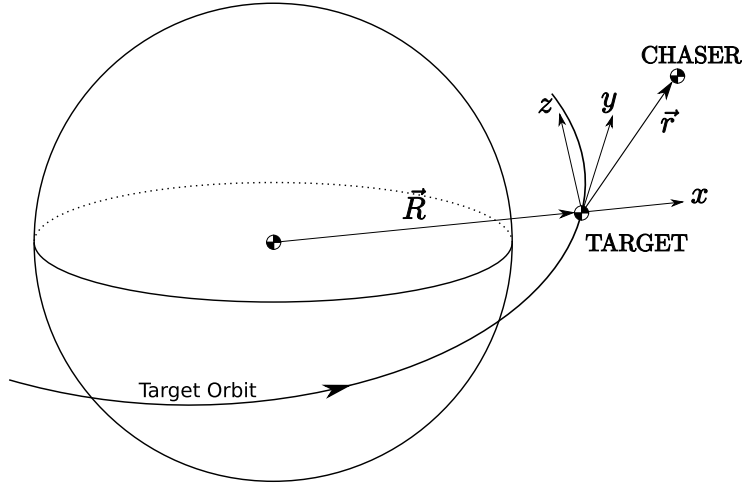


Figure 2: LVLH frame.

centric anomaly E . The time t_p is chosen such that it is equal or less than the starting time which is denoted as t_0 (subtracting, if necessary, any number of orbital periods). Kepler's equation is not analytically invertible, but its inverse can be found numerically with any desired degree of precision (see any Orbital Mechanics reference, such as Wie (1998)). Denote its inverse by the function K , i.e. $E = K(t)$. Denote by E_0 the true anomaly corresponding to t_0 , this is, $E_0 = K(t_0)$. Then, $E_k = K(t_k) = K(t_0 + kT)$, where T is the sampling time (not to be confused with the orbital period). Call as $r_{x,k}$, $r_{y,k}$, and $r_{z,k}$ the position of the chaser in a local-vertical/local-horizontal (LVLH) frame of reference fixed on the center of gravity of the target vehicle at time t_k . In the (elliptical) LVLH frame, x refers to the radial position, z to the out-of-plane position (in the direction of the orbital angular momentum), and y is perpendicular to these coordinates (not necessarily aligned with the target velocity given that its orbit is not circular). The velocity and inputs of the chaser in the LVLH frame at time t_k are denoted, respectively, by $v_{x,k}$, $v_{y,k}$, and $v_{z,k}$, and by $u_{x,k}$, $u_{y,k}$, and $u_{z,k}$.

If there is no actuation (i.e. $u_{x,k} = u_{y,k} = u_{z,k} = 0$), the resulting transition

equation was obtained in a simple form in Yamanaka and Ankersen (2002) as follows:

$$x_{k+1} = \Phi(t_{k+1}, t_k)x_k \quad (65)$$

where

$$x_k = [r_{x,k} \ r_{y,k} \ r_{z,k} \ v_{x,k} \ v_{y,k} \ v_{z,k}]^T, \quad (66)$$

and where

$$\Phi(t_{k+1}, t_k) = Y_{K(t_{k+1})}Y_{K(t_k)}^{-1}, \quad (67)$$

with Y_{t_k} being the fundamental matrix solution of the Tschauner-Hempel model, which are expressed in Yamanaka and Ankersen (2002) as a function of *true* anomaly θ . However there is a one-to-one relation between E and θ given by

$$\tan \frac{\theta}{2} = \sqrt{\frac{1+e}{1-e}} \tan \frac{E}{2}, \quad (68)$$

which is exploited in the sequel. The explicit expression of the matrices¹ is found in (69) and (70),

$$Y_E = \begin{bmatrix} s & 0 & 0 & 2/\rho - 3esJ & -c & 0 \\ c(1+1/\rho) & 1/\rho & 0 & -3\rho J & s(1+1/\rho) & 0 \\ 0 & 0 & c/\rho & 0 & 0 & s/\rho \\ \alpha\rho^2c & 0 & 0 & \alpha(-es - 3e\rho^2Jc) & \alpha\rho^2s & 0 \\ \alpha s(-1 - \rho^2) & \alpha es & 0 & \alpha\rho(3es\rho J - 3) & \alpha(c + e + c\rho^2) & 0 \\ 0 & 0 & -s\alpha & 0 & 0 & (c + e)\alpha \end{bmatrix}, \quad (69)$$

¹These expressions slightly differ from Yamanaka and Ankersen (2002) because the two transformation matrices that appear in that paper have been pre-multiplied; also, the reference axes are not the same.

$$\begin{aligned}
Y_E^{-1} &= \frac{3J}{(1-e^2)} \begin{bmatrix} e\rho^2(1+\rho) & -e^2\rho^2s & 0 & e^2s/\alpha & e\rho/\alpha & 0 \\ \rho^2(1+\rho) & -e\rho^2s & 0 & es/\alpha & \rho/\alpha & 0 \\ 0 & 0 & 0 & 0 & 0 & 0 \\ 0 & 0 & 0 & 0 & 0 & 0 \\ 0 & 0 & 0 & 0 & 0 & 0 \\ 0 & 0 & 0 & 0 & 0 & 0 \end{bmatrix} + \frac{1}{(1-e^2)} \\
&\times \begin{bmatrix} -s(\rho^2+2\rho+e^2) & es^2(1+\rho) & 0 & \frac{c-2e/\rho}{\alpha} & -\frac{s(\rho+1)}{\rho\alpha} & 0 \\ -es(1+\rho)^2 & \rho^2(1-ce)+e^2s^2 & 0 & \frac{ec-2/\rho}{\alpha} & -\frac{es(\rho+1)}{\rho\alpha} & 0 \\ 0 & 0 & (c+e)(1-e^2) & 0 & 0 & \frac{-s(1-e^2)}{\alpha\rho} \\ \rho^2(1+\rho) & -es\rho^2 & 0 & \frac{es}{\alpha} & \frac{\rho}{\alpha} & 0 \\ 3\rho(c+e)-e\rho s^2 & -esc(1+\rho)-e^2s & 0 & \frac{s}{\alpha} & \frac{c(\rho+1)+e}{\alpha\rho} & 0 \\ 0 & 0 & s(1-e^2) & 0 & 0 & \frac{c(1-e^2)}{\alpha\rho} \end{bmatrix} \quad (70)
\end{aligned}$$

where the following symbols are used (expressed in terms of E):

$$\rho = \frac{1-e^2}{1-e\cos E}, \quad s = \frac{\sqrt{1-e^2}\sin E}{1-e\cos E}, \quad c = \frac{\cos E - e}{1-e\cos E}, \quad (71)$$

$$J = \alpha \frac{E - \hat{E} - e(\sin E - \sin \hat{E})}{(1-e^2)^{3/2}}, \quad \alpha = \frac{n}{(1-e^2)^{3/2}}, \quad (72)$$

where \hat{E} in (72) can be substituted by zero or any other desired reference value of E . For instance, if when evaluating (67) one chooses $\hat{E} = E_k = K(t_k)$, then for $Y_{K(t_k)}^{-1}$ one gets $J = 0$ and the first matrix in (70) becomes zero.

Using (67), one gets A_k in (16) explicitly, as well as B_k in the impulsive case (explicitly defined in terms of $\Phi(t_{k+1}, t_k)$). To obtain the B_k matrix in the PWM and PAM cases, one needs to solve (8) or (12), respectively, which involves an integral. Defining

$$b_i(r_1, r_2, r_3) = \int_{r_1}^{r_2} \Phi(r_3, s) B_i(s) ds, \quad (73)$$

one has that, from (8),

$$B_{k,i}^W(\tau_{k,i}, \kappa_{k,i}) = b_i(t_k + \tau_{k,i}, t_k + \tau_{k,i} + \kappa_{k,i}, t_{k+1}), \quad (74)$$

and, from (12),

$$B_{k,i}^A = b_i(t_k, t_{k+1}, t_{k+1}). \quad (75)$$

To compute the b_i 's, the following integral is needed

$$\int Y_{K(t)}^{-1} C_{i+3} dt, \quad (76)$$

where C_i is a 6-element column vector of zeros with a value of one at row i . For the computation, define the functions $f_i(t)$, for $i = 1, 2, 3$, as the indefinite integrals of (76), in terms of eccentric anomaly

$$f_i(E) = \int Y_E^{-1} C_{i+3} \frac{1 - e \cos E}{n} dE. \quad (77)$$

Once the f_i 's are computed, one finds the b_i 's as

$$b_i(r_1, r_2, r_3) = Y_{K(r_3)} (f_i(K(r_2)) - f_i(K(r_1))) \quad (78)$$

Inserting the expression of (70) in (77) and integrating, one obtains

$$f_1 = \frac{(1 - e^2)^{-7/2}}{2\alpha^2} \begin{bmatrix} 2(1 + 6e^2)S - 3e(2 + e^2)E + e^2Ch + e^3\hat{S}/2 \\ 2e(8 - e^2)S - (4 + 7e^2 - 2e^4)E + eCh + e^2\hat{S}/2 \\ 0 \\ -2eC(1 - e^2)^{3/2} \\ -2C(1 - e^2)^{3/2} \\ 0 \end{bmatrix}, \quad (79)$$

$$f_2 = \frac{(1 - e^2)^{-3}}{2\alpha^2} \begin{bmatrix} C(4(1 + e^2) - eC) - eEh - 3eE^2 \\ eC(10 - 2e^2 - eC) - Eh - 3E^2 \\ 0 \\ 2E(1 - e^2)^{3/2} \\ \sqrt{1 - e^2}(4S - e(3E + \hat{S}/2)) \\ 0 \end{bmatrix}, \quad (80)$$

$$f_3 = \frac{(1 - e^2)^{-5/2}}{4\alpha^2} \begin{bmatrix} 0 \\ 0 \\ 2\sqrt{1 - e^2}C(2 - eC) \\ 0 \\ 0 \\ 4(e^2 + 1)S - e(6E + \hat{S}) \end{bmatrix}, \quad (81)$$

where $S = \sin(E)$, $\hat{S} = \sin(2E)$, $C = \cos E$, $h = 6\alpha(\hat{E} - E - e \sin(\hat{E}))$. Similar expressions for the B matrices can be found in Ankersen (2010), however using a slightly different definition of reference axes.

Note that, using these formulas, it is possible to express (16) explicitly for all actuation types. This greatly speeds up the algorithms.

6.1. Constraints for the rendezvous problem

Besides the input constraints (which were given in Section 3.1.2), the inequality state constraints which were generically specified in Section 3.1.1 are,

in general, related to safety and sensing considerations (see e.g. Breger and How (2008)). In this work, it is considered that during rendezvous the chaser vehicle has to remain inside a line of sight (LOS) area. To simplify the constraint², in this work a 2-D LOS area is used as shown in Figure 3. This LOS region is the intersection of a cone, given by the equations $r_y \geq c_{LOS}(r_x - r_{x_0})$ and $r_y \geq -c_{LOS}(r_x + r_{x_0})$, and the region $r_y \geq 0$.

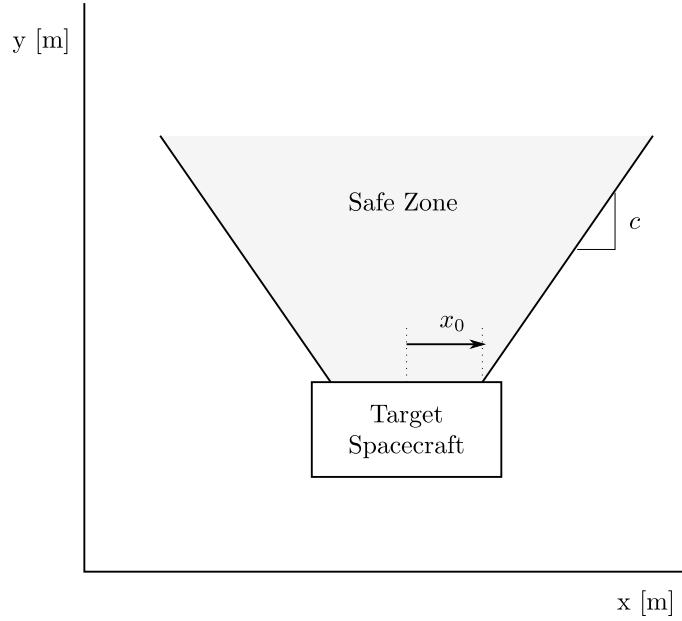


Figure 3: Line of Sight region.

The LOS constraint is $A_{LOS}x_k \leq b_{LOS}$, where

$$A_{LOS} = \begin{bmatrix} 0 & -1 & 0 & 0 & 0 & 0 \\ c_{LOS} & -1 & 0 & 0 & 0 & 0 \\ -c_{LOS} & -1 & 0 & 0 & 0 & 0 \end{bmatrix}, \quad b_{LOS} = \begin{bmatrix} 0 \\ c_{LOS}r_{x_0} \\ c_{LOS}r_{x_0} \end{bmatrix}. \quad (82)$$

Using the compact formulation that was developed in Section 2, the con-

²More complicated constraints could be considered, see Gavilan et al. (2012) for examples including a rotating LOS constraint.

straints equations for the state can be rewritten as:

$$A_c \mathcal{X} \leq b_c, \quad (83)$$

where A_c and b_c are given by:

$$A_c = \begin{bmatrix} A & & & \\ & A & & \\ & & \ddots & \\ & & & A \end{bmatrix}, b_c = \begin{bmatrix} b_{LOS} \\ b_{LOS} \\ \vdots \\ b_{LOS} \end{bmatrix}. \quad (84)$$

Then, using equation (20), one can reformulate the LOS constraints as constraints for the control signals, starting at time step t_k , in the following way:

$$A_c G_k \mathcal{U}_k \leq b_c - A_c F_k x_0. \quad (85)$$

7. Simulation Results

For simulations the following values have been used: $N_p = 50$ as planning horizon, $T = 60$ s, and $\bar{u} = 10^{-1}$ N/kg. The target orbit has $e = 0.7$ and perigee altitude $h_p = 500$ km. Initial conditions were $\theta_0 = 45^\circ$, $\mathbf{r}_0 = [0.25 \ 0.4 \ -0.2]^T$ km, $\mathbf{v}_0 = [0.005 \ -0.005 \ -0.005]^T$ km/s. The LOS constraint (see Vazquez et al. (2011)) is defined by $x_0 = 0.001$ km and $C_{LOS} = \tan 30^\circ$. For the cost function, α has been set to 10^3 and Q_k as

$$Q_k = \begin{bmatrix} R_{k+1} & & \\ & \ddots & \\ & & R_{k+N_p} \end{bmatrix}, \quad (86)$$

where R_k is defined as

$$R_k = h(k - k_a) \begin{bmatrix} \text{Id}_{3 \times 3} & \Theta_{3 \times 3} \\ \Theta_{3 \times 3} & \Theta_{3 \times 3} \end{bmatrix}. \quad (87)$$

In (87), h is the step function, k_a is the desired arrival time for rendezvous, and $\text{Id}_{3 \times 3}$, $\Theta_{3 \times 3}$ are respectively the identity matrix and a matrix full of zeros, both of order 3 by 3. The reason for choosing (87) is that it is desired to arrive at

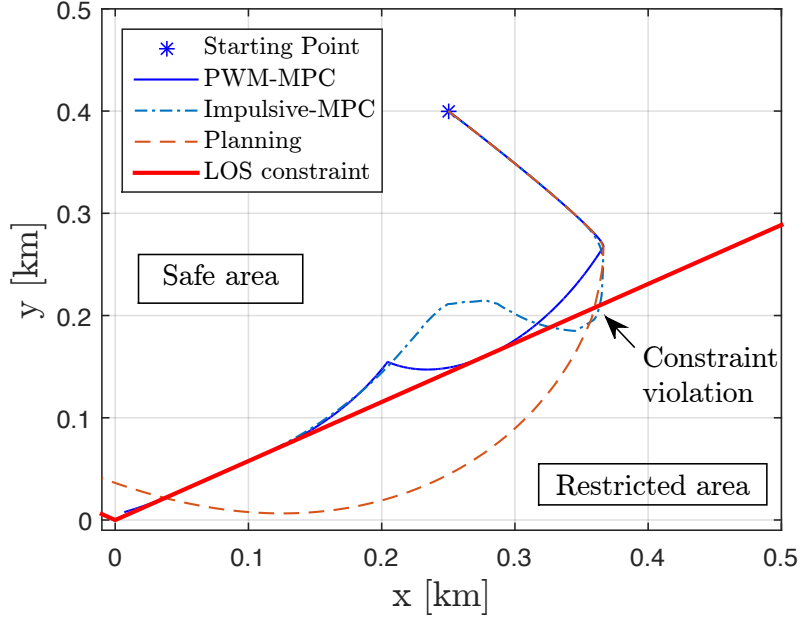


Figure 4: System trajectories in the target orbital plane: open-loop PWM inputs computed from impulsive solution (dashed), closed-loop Model Predictive Control with PWM inputs using impulsive model (dot-dashed), and closed-loop Model Predictive Control with PWM inputs using the PWM planning algorithm (solid).

the origin at time k_a (and *remain* there) and at the same time minimize the control effort.

In the simulations three algorithms were considered: first, an impulsive open-loop trajectory planner, as described in Section 4.1. Next, closed-loop simulations using MPC but considering impulsive instead of PWM actuation in the model (this algorithm is denoted as impulsive MPC). Finally, closed-loop simulations using MPC, based on the PWM algorithms as explained in Section 5. The impulses produced by the first and second methods are subsequently transformed to PWM inputs using the algorithm of Section 4.2.

Compare first the algorithms without disturbances. The trajectories (projected on the target orbital plane) are shown in Fig. 4. The open-loop impulsive

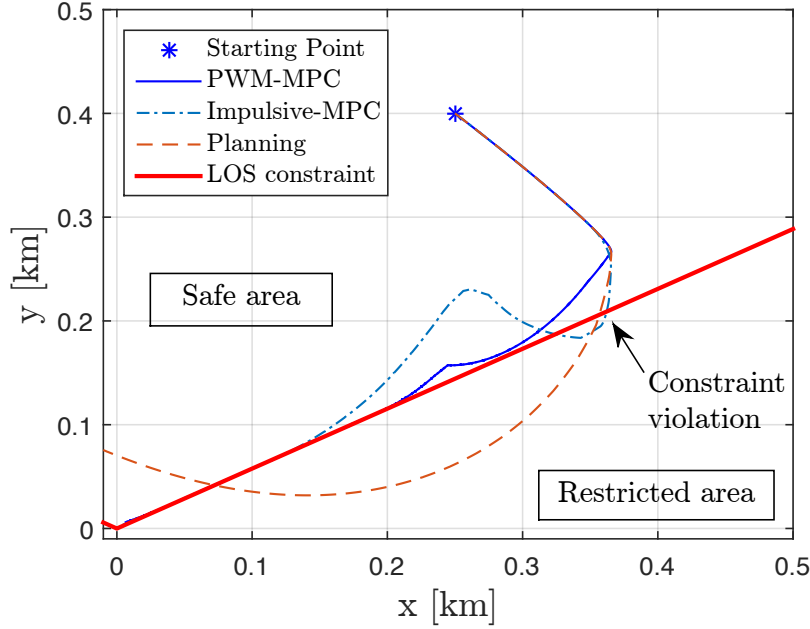


Figure 5: System trajectories in the target orbital plane, with inexact orbit model: open-loop PWM inputs computed with the planning algorithm (dashed), closed-loop Model Predictive Control with PWM inputs using impulsive model (dot-dashed), and closed-loop Model Predictive Control with PWM inputs using the PWM planning algorithm (solid).

solution does not achieve rendezvous and drifts away, whereas the other solutions successfully reach the origin (the simulation is stopped when the chaser vehicle was 5 meters or less away from the target). The impulsive MPC is able to mostly compensate its imperfect thruster model. The PWM MPC algorithm had a cost of 15.0 m/s and the impulsive MPC had a cost of 15.8 m/s. Thus, while a basic MPC is able to rendezvous, the use of an imperfect model has some fuel costs. In addition, the impulsive MPC does not satisfy the line-of-sight constraints for a period of time.

Next, Fig. 5 shows a simulation where the real orbit is different from the reference orbit used in the model (the real eccentricity is $e = 0.83$, the real perigee altitude is $h_p = 525$ km, and the real $\theta_0 = 60^\circ$). Both MPC algorithms

reach the origin (as in the previous scenario, the simulation is stopped when the chaser vehicle was 5 meters or less away from the target). The impulsive MPC again exits the line-of-sight region. The cost for the PWM MPC algorithm was 15.3 m/s, whereas the impulsive MPC had a cost of 15.8 m/s.

Each iteration took less than half a second on a conventional computer, using MATLAB and the *Gurobi* optimization package (see Gurobi Optimization, Inc. (2014)). With a maximum number of iterations of 6, the computation time remained well below the interval sampling time.

8. Concluding Remarks

This paper has presented a MPC algorithm that computes optimal PWM inputs for LTV systems. The algorithm is based on an initial approximation with either PAM or impulsive inputs, followed by iterative explicit linearization. As an application, the problem of rendezvous in elliptical orbits has been considered. In particular, the algorithm might be particularly useful for satellites with small specific thrust. The algorithm improves the fuel cost of an impulsive-only MPC (with the impulses posteriorly transformed to PWM inputs), and is able to satisfy safety constraints and handle disturbances such as imperfect knowledge of the target's orbit. This algorithm would help avoiding having to include a PWM approximation term in the "uncertainty budget" and therefore save costs. However, inclusion of real-life constraints and more realistic simulations are needed to validate the method.

Possible future lines of research include studying the convergence of the planning algorithm, guaranteeing constraint satisfaction by including an estimate of linearization error in the model, or analyzing the stability guarantees of the MPC design.

Acknowledgments

The authors acknowledge financial support of the Spanish Ministry of Science and Innovation under grant DPI2008-05818.

References

References

- Ankersen, F., 2010. Guidance, navigation, control and relative dynamics for spacecraft proximity maneuvers. Ph.D. thesis.
- Arzelier, D., Kara-Zaitri, M., Louembet, C., Delibasi, A., 2011. Using polynomial optimization to solve the fuel-optimal linear impulsive rendezvous problem. *J. Guid. Contr. Dynam.* 34, 1567–1572.
- Arzelier, D., Louembet, C., Rondepierre, A., Kara-Zaitri, M., 2013. A new mixed iterative algorithm to solve the fuel-optimal linear impulsive rendezvous problem. *J. Opt. Theor. Appl.* 159, 210–230.
- Asawa, S., Nagashio, T., Kida, T., 2006. Formation flight of spacecraft in earth orbit via MPC. In: SICE-ICASE International Joint Conference.
- Bernelli-Zazzera, F., Mantegazza, P., Nurzia, V., 1998. Multi-pulse-width modulated control of linear systems. *J. Guid. Contr. Dynam.* 21 (1), 64–70.
- Breger, L., How, J. P., 2008. Safe trajectories for autonomous rendezvous of spacecraft. *J. Guid. Contr. Dynam.* 31 (5), 1478–1489.
- Camacho, E., Bordons, C., 2004. Model Predictive Control, 2nd Edition. Springer-Verlag, pp. 131–205.
- Carter, T. E., 1998. State transition matrices for terminal rendezvous studies: Brief survey and new example. *J. Guid. Contr. Dynam.* 21 (1), 148–155.
- Clohessy, W. H., Wiltshire, R. S., 1960. Terminal guidance systems for satellite rendezvous. *J. Aerosp. Sc.* 27 (9), 653–658.
- D’Amico, S., Ardaens, J.-S., Gaias, G., Benninghoff, H., Schlepp, B., Jörgensen, J. L., 2013. Noncooperative rendezvous using angles-only optical navigation: System design and flight results. *Journal of Guidance, Control, and Dynamics* 36 (6), 1576–1595.

- Deaconu, G., Louembet, C., Théron, A., 2014. Minimizing the effects of the navigation uncertainties on the spacecraft rendezvous precision. *Journal of Guidance, Control, and Dynamics* 37 (2), 695–700.
- Deaconu, G., Louembet, C., Théron, A., 2015. Designing continuously constrained spacecraft relative trajectories for proximity operations. *Journal of Guidance, Control, and Dynamics* 38 (7), 1208–1217.
- Fehse, W., 2003. *Automated Rendezvous and Docking of Spacecraft*. Cambridge University Press.
- Gaias, G., D’Amico, S., Ardaens, J.-S., 2014. Angles-only navigation to a noncooperative satellite using relative orbital elements. *Journal of Guidance, Control, and Dynamics* 37 (2), 439–451.
- Gavilan, F., Vazquez, R., Camacho, E. F., 2009. Robust model predictive control for spacecraft rendezvous with online prediction of disturbance bound. In: *Proceedings of AGNFCS’09, Samara, Russia*.
- Gavilan, F., Vazquez, R., Camacho, E. F., 2012. Chance-constrained model predictive control for spacecraft rendezvous with disturbance estimation. *Contr. Eng. Pract.* 20 (2), 111–122.
- Gurobi Optimization, Inc., 2014. *Gurobi optimizer reference manual*.
URL <http://www.gurobi.com>
- Hartley, E. N., Trodden, P. A., Richards, A. G., Maciejowski, J. M., 2012. Model predictive control system design and implementation for spacecraft rendezvous. *Control Engineering Practice* 20 (7), 695 – 713.
- Hill, G., 1878. Researches in lunar theory. *American Journal of Mathematics* 1 (3), 5–26, 129–147, 245–260.
- Humi, M., Carter, T., 2008. Orbits and relative motion in the gravitational field of an oblate body. *J. Guid. Contr. Dynam.* 31 (3), 522–532.

- Ieko, T., Ochi, Y., Kanai, K., 1999. New design method for pulse-width modulation control systems via digital redesign. *J. Guid. Contr. Dynam.* 22 (1), 123–128.
- Inalhan, G., Tillerson, M., How, J. P., 2002. Relative dynamics and control of spacecraft formations in eccentric orbits. *J. Guid. Contr. Dynam.* 25 (1), 48–59.
- Jewison, C., Erwin, R. S., Saenz-Otero, A., 2015. Model predictive control with ellipsoid obstacle constraints for spacecraft rendezvous. In: *ACNAAV 2015 IFAC workshop*.
- Kim, H. J., Shim, D. H., Sastry, S., 2002. Nonlinear model predictive tracking control for rotorcraft-based unmanned aerial vehicles. In: *Proceedings of ACC 2002*.
- Larsson, R., Berge, S., Bodin, P., Jönsson, U., 2006. Fuel efficient relative orbit control strategies for formation flying and rendezvous within prisma. In: *Proceedings of the 29th AAS guidance and control conference*.
- Leomanni, M., Rogers, E., Gabriel, S. B., 2014. Explicit model predictive control approach for low-thrust spacecraft proximity operations. *Journal of Guidance, Control, and Dynamics* 37 (6), 1780–1790.
- Loumbet, C., Arzelier, A., Deaconu, G., 2015. Robust rendezvous planning under maneuvering errors. *Journal of Guidance, Control, and Dynamics* 38 (1), 76–93.
- Richards, A. G., How, J., 2003. Performance evaluation of rendezvous using model predictive control. *AIAA Paper 2003-5507*.
- Rossi, M., Lovera, M., 2002. A multirate predictive approach to orbit control of small spacecraft. In: *Proceedings of ACC 2002*.
- Rugh, W. J., 1996. *Linear System Theory (2Nd Ed.)*. Prentice-Hall, Inc., Upper Saddle River, NJ, USA.

- Shieh, L.-S., Wang, W.-M., Sunkel, J., 1996. Design of PAM and PWM controllers for sampled-data interval systems. *J Dyn Syst Meas Contr.* 118 (4), 673–681.
- Sinclair, A. J., Sherrill, R. E., Lovell, T. A., 2014. Calibration of linearized solutions for satellite relative motion. *Journal of Guidance, Control, and Dynamics* 37 (4), 1362–1367.
- Tschauner, J., Hempel, P., 1965. Rendezvous zu einem in elliptischer bahn umlaufenden. Ziel. *Acta Astronaut.* II (2), 104–109.
- Vazquez, R., Gavilan, F., Camacho, E. F., 2011. Trajectory planning for spacecraft rendezvous with on/off thrusters. In: *Proc. of IFAC World Congress 2011.*
- Vazquez, R., Gavilan, F., Camacho, E. F., 2014. Trajectory planning for spacecraft rendezvous in elliptical orbits with On/Off thrusters. In: *IFAC World Congress, Cape Town.*
- Vazquez, R., Gavilan, F., Camacho, E. F., 2015. Model predictive control for spacecraft rendezvous in elliptical orbits with On/Off thrusters. In: *ACNAAV 2015 IFAC workshop.*
- Weiss, A., Kolmanovsky, I., Baldwin, M., Erwin, R. S., 2012. Model predictive control of three dimensional spacecraft relative motion. In: *American Control Conference (ACC), 2012. IEEE*, pp. 173–178.
- Wie, B., 1998. *Space vehicle dynamics and control.* AIAA.
- Yamanaka, K., Ankersen, F., 2002. New state transition matrix for relative motion on an arbitrary elliptical orbit. *J. Guid. Contr. Dynam.* 25 (1), 60–66.

List of Figure Captions

1	PWM Variables.	6
2	LVLH frame.	21
3	Line of Sight region.	25
4	System trajectories in the target orbital plane: open-loop PWM inputs computed from impulsive solution (dashed), closed-loop Model Predictive Control with PWM inputs using impulsive model (dot-dashed), and closed-loop Model Predictive Control with PWM inputs using the PWM planning algorithm (solid).	27
5	System trajectories in the target orbital plane, with inexact orbit model: open-loop PWM inputs computed with the planning algorithm (dashed), closed-loop Model Predictive Control with PWM inputs using impulsive model (dot-dashed), and closed-loop Model Predictive Control with PWM inputs using the PWM planning algorithm (solid).	28